Clim. Past, 10, 975–985, 2014
www.clim-past.net/10/975/2014/
doi:10.5194/cp-10-975-2014

Climate of the Past
Open Access

Evaluation of the ability of the Chinese stalagmite $\delta^{18}O$ to record the variation in atmospheric circulation during the second half of the 20th century

S. Nan[1], M. Tan[2], and P. Zhao[1,3]

[1]Chinese Academy of Meteorological Sciences, Beijing, 100081, China
[2]Key Laboratory of Cenozoic Geology and Environment, Institute of Geology and Geophysics, Chinese Academy of Sciences, Beijing, 100029, China
[3]State Key Laboratory of Severe Weather, Chinese Academy of Meteorological Sciences, Beijing, 100081, China

Correspondence to: S. Nan (nansl@cams.cma.gov.cn) and M. Tan (tanming@mail.iggcas.ac.cn)

Received: 8 June 2013 – Published in Clim. Past Discuss.: 29 July 2013
Revised: 17 December 2013 – Accepted: 10 April 2014 – Published: 21 May 2014

Abstract. The Chinese stalagmite $\delta^{18}O$ ($\delta^{18}O_{cs}$) has provoked debate worldwide over the past few years due to its lack of quantitative calibration, leading us to questions of whether $\delta^{18}O_{cs}$ records a local or large-scale signal and whether $\delta^{18}O_{cs}$ records the signal of a single remote water vapor source or multiple water vapor sources. In this study, we observe all of the $\delta^{18}O_{cs}$ trends within the instrumental period to verify whether they possess a common trend, which could be used as a basis to determine whether the trends reflect the large-scale signal together or whether each trend reflects the local signal. The results show that most of the $\delta^{18}O_{cs}$ experienced a linear increase from 1960 to 1994, which may indicate that the $\delta^{18}O_{cs}$ could record a trend occurring in large-scale atmosphere circulations. We then quantitatively describe the proportion of water vapor transport (WVT) from different source regions. Using the NCEP/NCAR (National Centers for Environmental Protection/National Center for Atmospheric Research) reanalysis data from 1960 to 1994, the ratios of the intensities of three WVTs from the Bay of Bengal, the South China Sea, and the western North Pacific during the summer are calculated. We define $R_{SCS/BOB}$ as the ratio of the WVT intensities from the South China Sea to those from the Bay of Bengal, $R_{WNP/BOB}$ as the ratio of the WVT intensities from the western North Pacific to those from the Bay of Bengal, and $R_{WNP/SCS}$ as the ratio of the WVT intensities from the western North Pacific to those from the South China Sea. The significant decadal increase occurs in the time series of $R_{WNP/BOB}$ and $R_{WNP/SCS}$, most likely resulting from the strengthening of the WVT from the western North Pacific in the late 1970s due to the western Pacific subtropical high that extended westward. Further analysis indicates that when the equatorial central and eastern Pacific is in the El Niño phase, the sea surface temperature (SST) in the tropical Indian Ocean, the Bay of Bengal, and the South China Sea is high, and the SST at the middle latitudes in the North Pacific is low, then the $R_{WNP/BOB}$ and $R_{WNP/SCS}$ values tend to be high. After the late 1970s, the equatorial central and eastern Pacific have often been in the El Niño phase. Therefore, we confirm that the $\delta^{18}O_{cs}$ primarily records the variation in atmospheric circulation during the second half of the 20th century.

1 Introduction

The applications of absolutely dated oxygen isotope records from stalagmites in paleoclimate research have increased since the Chinese Hulu Cave record was published in the early 21st century (Wang et al., 2001). The signal of the oxygen isotope composition ($\delta^{18}O$) and, especially, the significance of the Chinese stalagmite $\delta^{18}O$ ($\delta^{18}O_{cs}$) have been widely discussed and argued (e.g., Maher, 2008; Maher and Thompson, 2012; Dayem et al., 2010; Clemens et al., 2010; Pausata et al., 2011; Lee et al., 2012). However, all of these authors suggest that the $\delta^{18}O_{cs}$ is primarily inherited from the precipitation $\delta^{18}O$ ($\delta^{18}O_p$). Therefore, a possible solution

to these debates depends on an understanding of the significance of the $\delta^{18}O_p$.

When water vapor condenses into liquid, $H_2^{18}O$ preferentially enters the liquid, whereas $H_2^{16}O$ is concentrated in the remaining vapor under constant temperature conditions because the zero-point energy of $H_2^{16}O$ is greater than that of $H_2^{18}O$ (O'Neil, 1986). As an air mass moves from a warm region to a cold region, water vapor condenses and is removed as precipitation. The phenomenon of a lower temperature causing the precipitation to have a lower $^{18}O/^{16}O$ ratio during the distillation processes is called the "temperature effect" (Dansgaard 1964). This principle also explains other important observations, such as the observation that $\delta^{18}O$ decreases with increasing precipitation rates due to the reduced evaporation of liquid condensate, which is the "amount effect". Seasonal changes in $\delta^{18}O_p$ resulting from the amount effect, first described by Dansgaard (1964), have been a starting point for isotope-related studies, including those highlighting the amount effect in China (e.g., Araguás-Araguás et al., 1998; Tian et al., 2003; Yamanaka et al., 2004; Johnson and Ingram, 2004). The amount effect has been historically related to the main property of $\delta^{18}O_p$ in the regions strongly affected by the summer monsoon. However, two main points mentioned by Dansgaard (1964) should be emphasized before using $\delta^{18}O_p$ as a tracer of the precipitation amount. First, the development of the concept of the amount effect was derived from monthly and even synoptic timescales. Second, the amount effect was presented based on the hypotheses that raindrop evaporation and isotopic equilibrium fractionation tend to increase $\delta^{18}O_p$ in small amounts of rain. An unchanged water source is a precondition for these assumptions. However, in certain areas, such as in the monsoon regions of China, the water vapor source and the transport pathways significantly change in different seasons or different years due to oscillations in the atmospheric circulation (Zheng et al., 2009; Liu et al., 2008, 2010).

Through certain special weather events, we can intuitively construct the relationships between the water vapor source and the isotope ratio values. For example, in August of 1997, typhoons (hurricanes) Victor and Zita, the only two tropical cyclones attacking Hong Kong that year, led to the highest monthly rainfall (829 mm), with the monthly $\delta^{18}O$ valued at -5.61 ‰ (VSMOW) in Hong Kong. In addition, it has been confirmed that tropical cyclone rainfall tends to be more depleted in the heavy isotope of oxygen (^{18}O) than typical summertime low- to mid-latitude rainfall (Kilbourne et al., 2012; Frappier, 2013). Therefore, the rainwater $\delta^{18}O$ value in August was expected to be extremely low considering the double negative bias resulting from the amount effect and the typhoons. However, comparing the case of August with the adjacent months, the rainfalls were 764 mm with the monthly $\delta^{18}O$ valued at -7.51 ‰ (VSMOW) in July and 233 mm with the monthly $\delta^{18}O$ valued at -10.21 ‰ (VSMOW) in September. The typhoon transports water vapor from the Pacific Ocean to the monsoon regions of China. Thus, this is only one account explaining the reason that the water vapor from the Pacific Ocean (local) is more enriched in ^{18}O than other sources from remote oceans. According to evidence at wider spatial scales, we further propose a hypothesis of the circulation effect (Tan, 2014). Based on the Rayleigh distillation equation (Rayleigh, 1896), the changes in the atmospheric–oceanic circulation can directly or indirectly affect the variation in the ratio of water vapor originating from remote oceans (becoming depleted in ^{18}O) and local oceans (relatively enriched in ^{18}O) to an observed site, resulting in the fluctuation of the $\delta^{18}O_p$ observed at this site. If our hypothesis is correct, then the $\delta^{18}O_p$ from many places in the monsoon regions of China mainly reflects neither the amount effect nor the strength of a single summer monsoon but rather the intensity contrast between two summer monsoons (the southwest monsoon and the southeast monsoon). Thus, a quantitative description of the relative intensity of the remote and local water vapor transport (WVT) becomes necessary.

The WVT is one of the most important components of the East Asian monsoon system. A large amount of water vapor is directly transported from the adjacent oceans to East Asia (Lau and Li, 1984; Tao and Chen, 1987; Jiang and Li, 2009). There are four WVT pathways directly entering into continental East Asia during the summer: (1) the southwesterly monsoon in the South China Sea transports the water vapor to continental East Asia; (2) the southeasterly air current on the west and southwest of the western Pacific subtropical high (WPSH) transports the water vapor from the western Pacific to continental East Asia; (3) the southwesterly summer monsoon directly transports the water vapor from the Bay of Bengal to continental East Asia; and (4) the westerly wind at the mid–high latitudes transports the water vapor to continental East Asia. Among the four WVT pathways, the pathway from the westerly wind at the mid–high latitudes is the weakest (therefore, it is ignored in the following analysis), and the other three pathways arise from oceans at low latitudes (Jiang and Li, 2009).

As an assumption, Tan (2009, 2014) recently presented that the changes in the $\delta^{18}O_{cs}$ and the $\delta^{18}O_p$ in the monsoon regions of China could reflect the variable ratio of the remote water vapor from the Indian Ocean and the local water vapor from the Pacific. However, there is no quantitative description for the ratio of the remote and local water vapor. One of the main objectives of this study is to reveal the relative intensity of the remote and local WVTs and the associated features of the atmospheric circulation. In addition, we attempt to examine the details of the changes in the $\delta^{18}O_{cs}$ during the instrumental period based on the assumption that the $\delta^{18}O_{cs}$ can be inherited from the $\delta^{18}O_p$, and we attempt to discover the response of $\delta^{18}O_{cs}$ to certain meteorological variables, including those newly obtained herein.

2 Data and methods

Our research involves published data from stalagmite isotope studies, meteorological observations and newly produced findings herein by the integration of other data.

Most of the published $\delta^{18}O_{cs}$ data are available from the NOAA (National Oceanic and Atmospheric Administration) website (http://www.ncdc.noaa.gov/data-access/paleoclimatology-data). For our purposes, only the series that extend into the observation period are selected. Considering that all of the data sets should match, we focus only on the time span from 1960 to 1994 (considering the available and convincing data). In addition, the selected sequence must have eight or more data sets because the average resolution of the selected sequence is required to be better than 5 years. The following seven sequences satisfy this requirement: S312 from Shihua Cave in Beijing (Li et al., 1998), D15 from Dongge Cave in Guizhou (He et al., 2005; data are provided by the first author), WX42B from Wanxiang Cave, HY3 from Huangye Cave in Gansu (Zhang et al., 2008; Tan et al., 2011), HS4 from Heshang Cave in Hubei (Hu et al., 2008), A1 from Lianhua Cave in Hunan (Cosford et al., 2008), and DY1 from Dayu Cave in Shanxi (Tan et al., 2009). Of these sequences, the S312 δ^{18}O time series is re-dated by annual layer counting with an approach of using the annual layer thickness of the same stalagmite (but numbered TS9501; data are available at the same website; see Tan et al., 2003, for details) to fit the distance from the isotope sub-sampling spot to the top of S312, whereas for the age control of the other sequences, the original data reported by the literature are used here. D15 has only one age control point with a large uncertainty within the mentioned period: 29 ± 58 year b2k, i.e., 1971 ± 58 AD; WX42B has two age control points with very small uncertainties: 1990 ± 1 AD and 1970 ± 1 AD; HY3 has a very poor age control: 2369 ± 457 AD; HS4 is age-controlled by annual layer counting; A1 has no age control point within the mentioned period; DY1 has two inseparable age control points with small uncertainties: 1970 ± 1 AD and 1969 ± 3 AD. Based on this analysis of the uncertainties, the series S312, WX42B, and HS4 could be trusted, whereas the others, especially A1 and HY3, can be used for reference only.

Global reanalysis data sets provided by NCEP/NCAR (National Centers for Environmental Protection/National Center for Atmospheric Research) from 1960 to 1994 are used to calculate the terms of the atmospheric WVT (Kalnay et al., 1996). The physical variables used in this study include the monthly specific humidity and the meridional and zonal wind components at eight standard pressure levels, namely, 1000, 925, 850, 700, 600, 500, 400, and 300 hPa. The geopotential heights at 850 and 500 hPa are used to describe the atmospheric circulation variation. The surface pressure is used to remove the topography influence. The monthly mean sea surface temperature (SST) from the Hadley Centre Sea Ice and Sea Surface Temperature data set (HadISST) from 1960 to 1994 is used in this study (Rayner et al., 2003). The NCEP/NCAR and HadISST data have horizontal resolutions of 2.5 and 1°, respectively.

The vertically integrated moisture flux can be expressed in the following equation:

$$\boldsymbol{Q} = \frac{1}{g}\int_{p_t}^{p_s} \boldsymbol{V}\, q \,\mathrm{d}p, \tag{1}$$

where $\boldsymbol{V}$ is the horizontal wind vector, q is the specific humidity, p_s is the lower boundary (here, the surface pressure), p_t is the upper boundary (here, 300 hPa), p is the pressure, and g is the acceleration due to gravity. Because the NCEP/NCAR reanalysis sets the specific humidity to zero above 300 hPa, the vertical integration of Eq. (1) is performed from the surface to 300 hPa. The missing data above 300 hPa have a nearly negligible influence on the result because of the concentration of the water vapor in the lower troposphere (Zhou, 2003). In addition, the horizontal wind vector, specific humidity, and surface pressure from the ERA-40 reanalysis data set are used to recalculate the vertically integrated moisture flux for comparison (see Sect. 6).

The analysis methods employed in this study include correlation and composite analyses. The Student t test is used to evaluate the statistical significance. Unless otherwise specified, the 95 % confidence level is used to measure a significant signal.

3 Results and analysis

3.1 The $\delta^{18}O_{cs}$ trend during the second half of the 20th century

Over the past decade, studies have shown that the millennial-timescale climate events, such as the Younger Dryas recorded by the $\delta^{18}O_{cs}$, possess similar characteristics over a relatively wide area in China as follows: from the southwestern to eastern China (i.e., Dongge Cave and Hulu Cave; see Yuan et al., 2004) and then to northern China (Ma et al., 2012). However, a recent simulation revealed that the precipitation amount in southern China was in anti-phase with that in northern China on the millennial scale (Liu et al., 2014). The modern meteorological observations also illustrate that the amount of precipitation in northern China varies inversely with that in the Yangtze River valley on decadal scales (Ding et al., 2008). Thus, an interesting query addresses the trend of the $\delta^{18}O_{cs}$ within the instrumental period and whether the $\delta^{18}O_{cs}$ in northern China is different from that in southern China if the $\delta^{18}O_{cs}$ responds to precipitation. In this study, we attempt to answer these questions according to the aforementioned $\delta^{18}O_{cs}$ data and by considering the suitability of climatic data. The $\delta^{18}O_{cs}$ profiles from 1960 to 1994 are shown in Fig. 1. Additionally, because the $\delta^{18}O_{cs}$ could be smoothed due to the mixing of precipitation events within the soil and

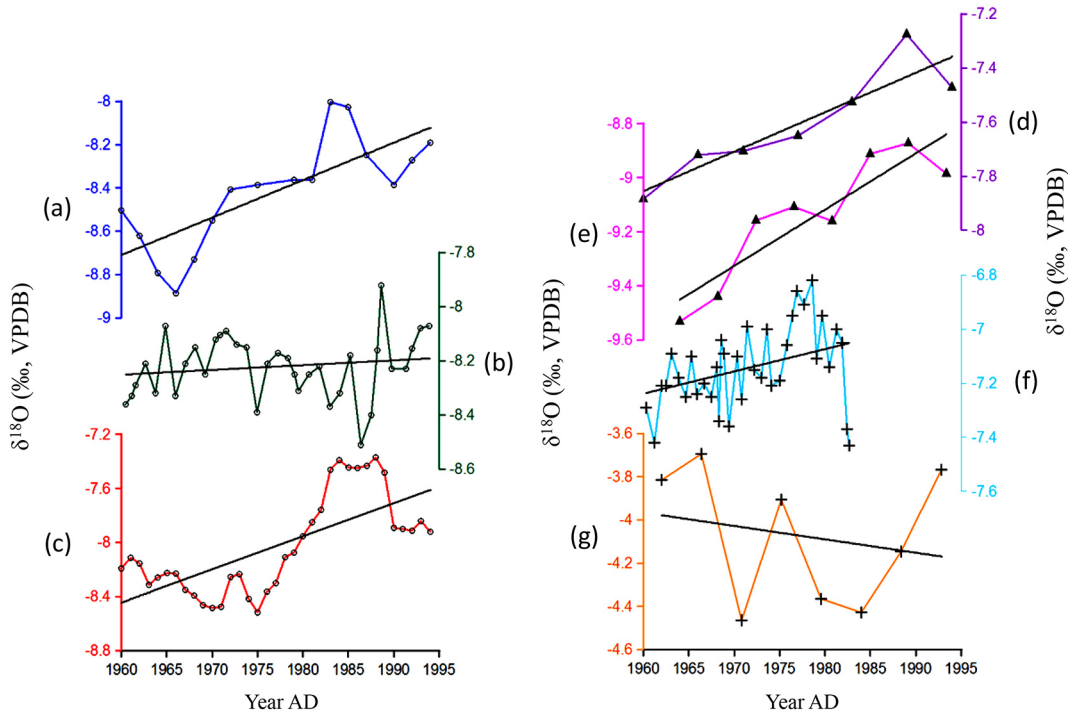

Figure 1. The trend estimation in the time series of the $\delta^{18}O_{cs}$ (1960–1994). Here, **(a)** is S312 from Shihua Cave, **(b)** is WX42B from Wanxiang Cave, **(c)** is HS4 from Heshang Cave, **(d)** is D15 from Dongge Cave, **(e)** is HY3 from Huangye Cave, **(f)** is DY1 from Dayu Cave, and **(g)** is A1 from Lianhua Cave (see text for details).

groundwater, the decadal trend may be the shortest-timescale variability that is worth considering.

As shown in Fig. 1, all of the series, except for A1 from Lianhua Cave (Fig. 1g), possess increasing trends; their trend equations, correlation coefficients, and confidence levels are listed in Table 1. As previously described, the series a, b and c (in Fig. 1 and Table 1) possess reliable age control, whereas the others could be used for reference only due to large dating errors (such as HY3) or no time control during the mentioned period (such as A1). However, the statistical analysis of the trends in these sequences indicates that most sequences share a common increasing trend during the period of interest.

According to modern meteorological observations, the northern China areas (such as Beijing, the nearest observation station to S312) and the area in the Yangtze River valley (e.g., Yichang, the nearest observation station to HS4) have opposite trends of precipitation and temperature (see Fig. S1 in the Supplement). Assuming that neither the temperature nor the precipitation causes the increasing trend, the ratio of the water vapor from local to remote oceans would most likely be responsible for the common increasing trend in the $\delta^{18}O_{cs}$. Therefore, the next step in our study is to analyze the intensities of the WVTs and their ratios in the period of interest.

Table 1. The trend equation and correlation coefficient for the $\delta^{18}O_{cs}$ (1960–1994).

Stalagmite numbered	Trend equation	Correlation coefficient	Confidence level
a: S312	$Y = 0.017\,X - 42.628$	$r = 0.76$	$p < 0.001$
b: WX42B	$Y = 0.002\,X - 11.710$	$r = 0.16$	$p < 0.5$
c: HS4	$Y = 0.025\,X - 56.476$	$r = 0.69$	$p < 0.001$
d: D15	$Y = 0.015\,X - 36.457$	$r = 0.91$	$p < 0.001$
e: HY3	$Y = 0.021\,X - 50.346$	$r = 0.90$	$p < 0.001$
f: DY1	$Y = 0.008\,X - 23.402$	$r = 0.37$	$p < 0.05$
g: A1	$Y = -0.006\,X + 8.149$	$r = -0.07$	$p > 0.5$

3.2 The time series for the intensity of the WVT

In this study, we primarily review the summer moisture transport in East Asia. Figure 2 shows the climatological mean WVT flux vectors vertically integrated during the summer from 1960 to 1994. There are three pathways of the WVTs from the oceans at low latitudes to East Asia. The first pathway is the southwesterly monsoon (Indian monsoon) transport, derived from the South Indian Ocean, crossing the Equator in Somalia, and passing over the Arabian Sea, the Bay of Bengal (a portion directly enters into China), the Indo-China Peninsula, and the South China Sea into the monsoon regions of China. The second pathway is

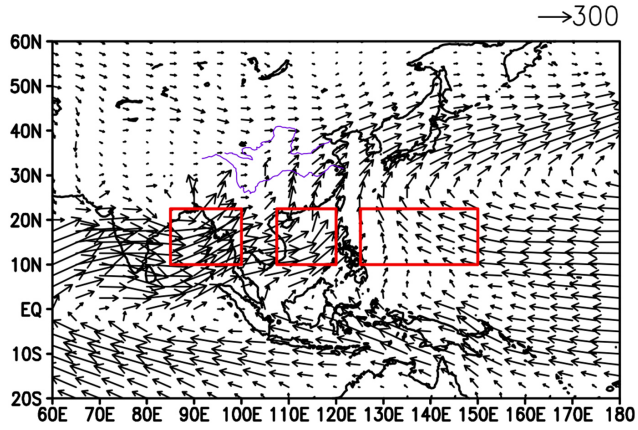

Figure 2. The climatological mean of summer (June-July-August) water vapor flux vectors vertically integrated from the surface to 300 hPa from 1960 to 1994 (unit: kg cm^{-1} s^{-1}); the three rectangles indicate the extents of the Bay of Bengal, the South China Sea, and the western North Pacific from left to right, successively.

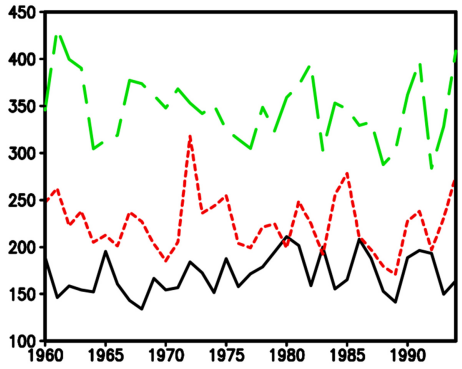

Figure 3. The time series of the WVT intensities from the western North Pacific (solid line; black), the South China Sea (short dotted line; red), and the Bay of Bengal (long dotted line; green) from 1960 to 1994. The units are kg cm^{-1} s^{-1}.

Table 2. The mean and standard deviation of the WVT intensities from the Bay of Bengal, the South China Sea, and the western North Pacific from 1960 to 1994. The unit is kg cm^{-1} s^{-1}.

	The Bay of Bengal	The South China Sea	The western North Pacific
Mean	347.2	225.0	171.0
Standard deviation	35.5	30.4	20.9

the Asian–Australian monsoon transport, which crosses the Equator and converges with the flow of the Indian monsoon at the South China Sea into China. The third pathway is the southeasterly monsoon transport, driving water vapor from the Pacific Ocean to the monsoon regions of China, in which the WPSH plays a major role. Therefore, the oceanic regions that directly transport the water vapor to East Asia are the Bay of Bengal, the South China Sea, and the western North Pacific. The regionally averaged moisture flux modes are defined to represent the following intensities of the WVTs: the intensity of the WVT from the western North Pacific (125–150° E; 10–22.5° N), the intensity of the WVT from the South China Sea (107.5–120° E; 10–22.5° N), and the intensity of the WVT from the Bay of Bengal (85–100° E; 10–22.5° N). The selected regions are in accord with those selected by Tian et al. (2004).

The time series of the intensities related to the three WVT pathways are illustrated in Fig. 3, all of which show the obvious interannual variations. The intensity of the WVT from the western North Pacific shows a significant increasing trend from 1960 to 1994. The intensity of the WVT from the Bay of Bengal is the strongest, and the intensity of the WVT from the South China Sea is slightly stronger than that from the western North Pacific (Table 2). For the standard deviations, the intensity of the WVT from the Bay of Bengal has the widest amplitude, and the intensity of the WVT from the South China Sea has a wider amplitude than that from the western North Pacific (Table 2). The mutual-correlation analyses show the independent relationship between the intensities of the WVT from the Bay of Bengal and the western North Pacific and between the intensities of the WVT from the South China Sea and the western North Pacific. There is a significant correlation between the intensities of the WVT from the Bay of Bengal and the South China Sea (their correlation coefficient is 0.53) due to the flow in the South China Sea, including one part of the southwesterly monsoon from the Bay of Bengal.

3.3 The time series for the ratios of the intensities of the WVTs

The ratios of the intensities of the WVTs are calculated here, and the shortened definitions are as follows: $R_{SCS/BOB}$ represents the ratio of the WVT intensities from the South China Sea and the Bay of Bengal, $R_{WNP/BOB}$ represents the ratio of the WVT intensities from the western North Pacific and the Bay of Bengal, and $R_{WNP/SCS}$ represents the ratio of the WVT intensities from the western North Pacific and the South China Sea. The $R_{SCS/BOB}$, $R_{WNP/BOB}$, and $R_{WNP/SCS}$ ratios are expected to reflect the relative intensities among the three WVTs. Figure 4 indicates the time series of the ratios from 1960 to 1994, showing that they all present an obvious interannual variation. Both $R_{WNP/BOB}$ and $R_{WNP/SCS}$ show a significant decadal increase, most likely resulting from the decadal increase of the WVT intensity from the western North Pacific, which is most likely responsible for the increasing trends in the $\delta^{18}O_{cs}$. The explanation for this trend is that the western North Pacific is a local water vapor source and the Bay of Bengal is a remote water vapor source for most of the monsoonal regions of China.

Table 3. The years of high and low $R_{SCS/BOB}$, $R_{WNP/BOB}$, and $R_{WNP/SCS}$.

	Years
High $R_{SCS/BOB}$	1960, 1972, 1975, 1984, 1985, 1993
Low $R_{SCS/BOB}$	1962, 1969, 1970, 1971, 1980, 1989
High $R_{WNP/BOB}$	1965, 1979, 1983, 1986, 1992, 1995
Low $R_{WNP/BOB}$	1959, 1961, 1962, 1963, 1967, 1968
High $R_{WNP/SCS}$	1980, 1983, 1986, 1987, 1992, 1995
Low $R_{WNP/SCS}$	1959, 1961, 1968, 1972, 1985, 1994

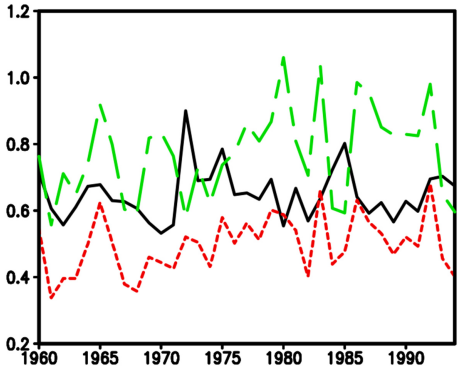

Figure 4. The time series of $R_{SCS/BOB}$ (solid line; black), $R_{WNP/BOB}$ (short dotted line; red), and $R_{WNP/SCS}$ (long dotted line; green) from 1960 to 1994.

4 Atmospheric circulations and the WVTs associated with the $R_{SCS/BOB}$, $R_{WNP/BOB}$, and $R_{WNP/SCS}$

To detect the atmospheric circulations and the WVTs associated with $R_{SCS/BOB}$, $R_{WNP/BOB}$,and $R_{WNP/SCS}$, we select the years with the highest and lowest $R_{SCS/BOB}$, $R_{WNP/BOB}$, and $R_{WNP/SCS}$ values (Table 3) to conduct the composite analysis. Figure 5a shows the composite differences of the 850 hPa geopotential height between the high- and low-$R_{SCS/BOB}$ years. The only small-scope anomaly in the western Pacific is above the 95% confidence level. In the 850 hPa horizontal winds (Fig. 6a), there are anomalous northeasterly winds from China to the Bay of Bengal; however, they are insignificant. There is an anomalous cyclonic circulation, on the west of which anomalous northerly winds appear over the northern part of the South China Sea, against the WVT from the South China Sea to China. The composite differences of the water vapor flux (Fig. 7a) reveal that the WVT from the Bay of Bengal to China weakens. However, the WVT from the South China Sea does not increase. Therefore, using $R_{SCS/BOB}$ to represent the relative intensity of the WVTs from the South China Sea and the Bay of Bengal to China is unsuitable. The infeasibility of using the methods in the study to obtain the variability of the relative intensity of the WVTs from the South China Sea and the Bay of Bengal to

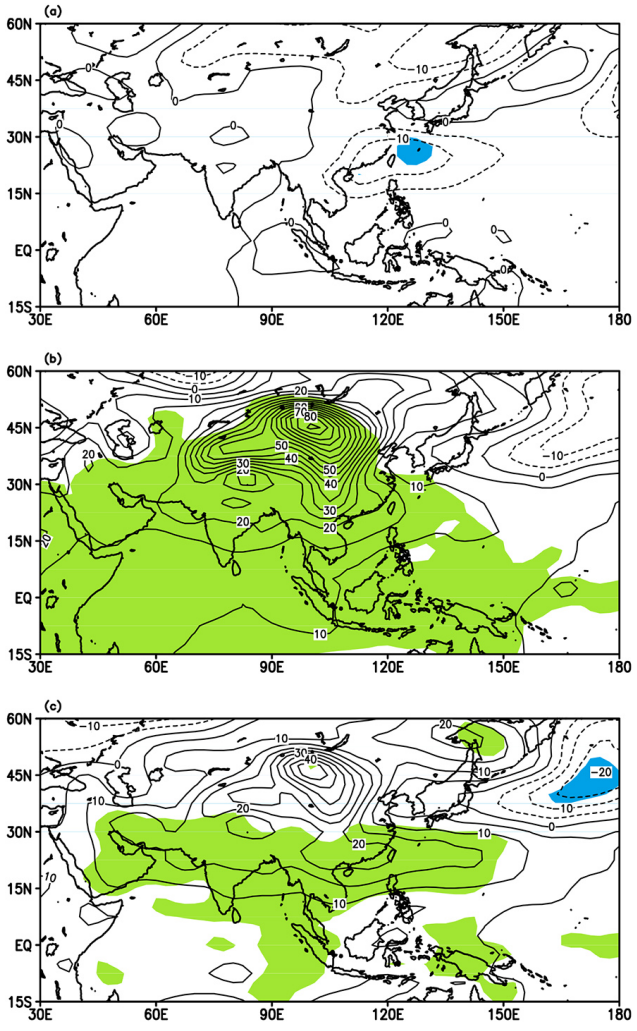

Figure 5. The composite differences of the summer 850 hPa geopotential height (m) between high and low $R_{SCS/BOB}$ **(a)**, $R_{WNP/BOB}$ **(b)**, and $R_{WNP/SCS}$ **(c)**. The shaded area is above the 95 % confidence level.

China might be because of their close relation. Therefore, we only focus on $R_{WNP/BOB}$ and $R_{WNP/SCS}$ below.

The composite difference of the 850 hPa geopotential height between the high- and low-$R_{WNP/BOB}$ years is shown in Fig. 5b. Continental East Asia and the western North Pacific are covered by positive values, indicating the weakened Asian low and the intensified WPSH. In 850 hPa horizontal winds (Fig. 6b), the anomalous easterly and southeasterly winds prevail over the south of the WPSH, indicating that the easterly and southeasterly winds in climatology increase. The anomalous northeasterly and easterly winds prevail from East Asia to the Bay of Bengal, indicating that the westerly and southwesterly winds in climatology decrease in these regions. In the corresponding moisture flux (Fig. 7b), there exists the anomalous westward WVT in the western North Pacific and the anomalous southwestward and westward WVT

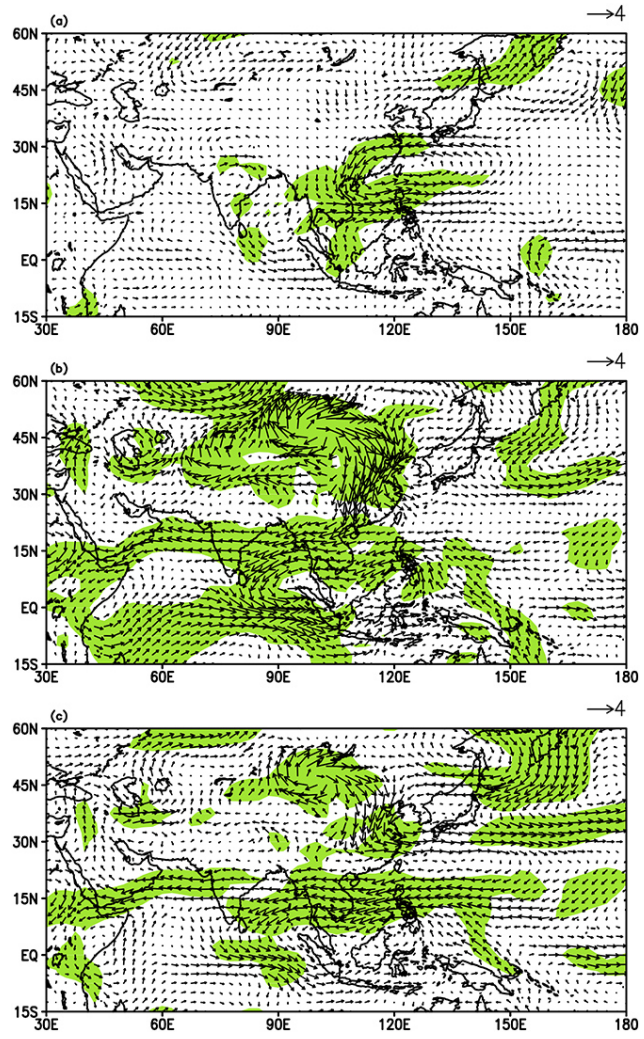

Figure 6. Same as Fig. 5 except for the 850 hPa horizontal wind vectors (m s^{-1}). The wind vectors above the 95 % confidence level are shaded.

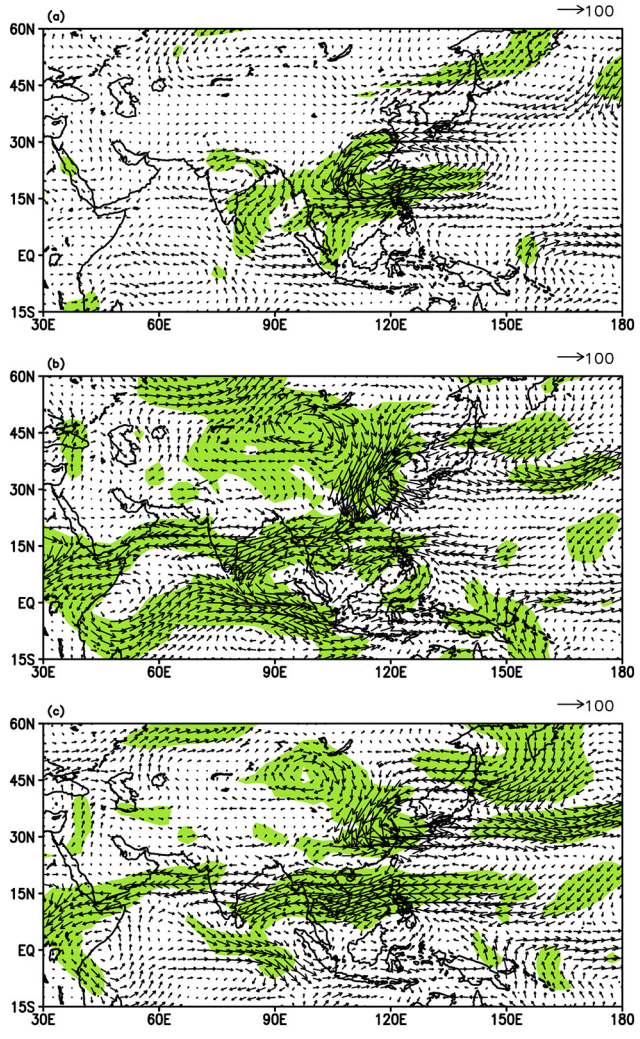

Figure 7. Same as Fig. 5 except for the moisture flux vectors vertically integrated from the surface to 300 hPa (kg cm^{-1} s^{-1}).

from East Asia to the Bay of Bengal, implying that the WVT from the south and southwest of the WPSH to East Asia in climatology increases, and the WVT from the Bay of Bengal to East Asia decreases. The contrasting relationship between the WVT from the Bay of Bengal and the western North Pacific to East Asia is consistent with the study by Zhang (2001). The 850 hPa geopotential height (Fig. 5c), horizontal wind (Fig. 6c), and the moisture flux (Fig. 7c) composites based on the $R_{\mathrm{WNP/SCS}}$ years are similar to those based on the $R_{\mathrm{WNP/BOB}}$ years. The Asian low weakens, and the WPSH strengthens. The anomalous easterly winds prevail over the south of the WPSH, implying that the WVT from the western North Pacific to East Asia strengthens. The anomalous northeasterly winds over the South China Sea are above the 95 % confidence level, indicating that the WVT from the South China Sea to East Asia weakens.

In general, a high (low) $R_{\mathrm{WNP/BOB}}$ may reflect the contrasting feature of the strong (weak) WVT from the western North Pacific and the weak (strong) WVT from the Bay of Bengal to East Asia. A high (low) $R_{\mathrm{WNP/SCS}}$ may reflect the contrasting feature of the strong (weak) WVT from the western North Pacific and the weak (strong) WVT from the South China Sea to East Asia.

The WPSH is important for the monsoon climate in East Asia. Therefore, the relationship between the WPSH and the $R_{\mathrm{WNP/BOB}}$ and $R_{\mathrm{WNP/SCS}}$ ratios is analyzed in this study. Figure 8 shows the positions of the WPSH for the high- and low-$R_{\mathrm{WNP/BOB}}$ and high- and low-$R_{\mathrm{WNP/SCS}}$ years, respectively. The positions of the WPSH are indicated with 5870 gpm in 500 hPa. The WPSH is located eastwards and diminishes in low $R_{\mathrm{WNP/BOB}}$ years compared with high $R_{\mathrm{WNP/BOB}}$ years (Fig. 8a). The west side is located at approximately 140° E for the low $R_{\mathrm{WNP/BOB}}$ years and at approximately 120° E for the high $R_{\mathrm{WNP/BOB}}$ years. The westward and strengthened

WPSH may lead more of the WVT from the western North Pacific to the Asian continent, in favor of heavier $\delta^{18}O_{cs}$, and vice versa. The positions and intensities of the WPSH for high- and low-$R_{WNP/SCS}$ years are similar to those for high- and low-$R_{WNP/BOB}$ years (Fig. 8b). The WPSH primarily affects the WVT from the western North Pacific to East Asia. Therefore, there is a close relationship between the WPSH and the $R_{WNP/BOB}$ and $R_{WNP/SCS}$ ratios. The WPSH has experienced an interdecadal-scale transition (Hu, 1997; Gong and He, 2002) and has enlarged, intensified, and shifted southwestward since the late 1970s. This observation is also in agreement with the decadal changes of the WVT intensity from the western North Pacific to East Asia, $R_{WNP/BOB}$ and $R_{WNP/SCS}$, and the $\delta^{18}O_{cs}$.

5 Mechanism analysis and the SST signal

Oceans are atmospheric moisture sources. The SST in certain crucial regions may locally and remotely affect the atmospheric circulations and further affect the WVT pathways and intensities. Because of the slow and persistent features of the ocean motion, signals of an atmospheric circulation anomaly can often be found in previous oceans. Tan (2014) reveals that the El Niño–Southern Oscillation (ENSO) cycle appears to be the dominant control of the interannual variation in the $\delta^{18}O_p$ in the monsoon regions of China. Therefore, we attempt to reveal whether there are relationships between the $R_{WNP/BOB}$ and $R_{WNP/SCS}$ ratios and the SST. Figure 9 shows the correlation maps of $R_{WNP/BOB}$ with the SST. The positive correlations appear over the equatorial central-eastern Pacific, the tropical Indian Ocean, the Bay of Bengal, and the western North Pacific from the previous winter to the concurrent summer. The negative correlations appear over the middle latitudes in the North Pacific from the previous autumn to this summer. These results indicate that the high summer $R_{WNP/BOB}$ values are associated with the El Niño phase in the equatorial central-eastern Pacific; the high SST in the tropical Indian Ocean, the Bay of Bengal, and the western North Pacific; and the low SST at the middle latitudes in the North Pacific in the previous autumn–winter. The correlation maps of $R_{WNP/SCS}$ with the SST (figure is not shown) are similar to those of $R_{WNP/BOB}$ with the SST. In Sect. 4, we conclude that $R_{WNP/BOB}$ is related to the position and intensity of the WPSH. Additionally, the correlation coefficient of the summer westward extension index of the WPSH (WPSHI; see Lu and Ye, 2010) and the averaged SST of February, March, and April in the El Niño 3.4 region is 0.56 at 99.9 % confidence levels. Wang et al. (2013) note that the WPSH variation is primarily controlled by the central Pacific cooling/warming and a positive atmosphere–ocean feedback between the WPSH and the Indo-Pacific warm pool oceans. Zhou et al. (2009) have suggested that the negative heating in the central and eastern tropical Pacific and increased convective heating in

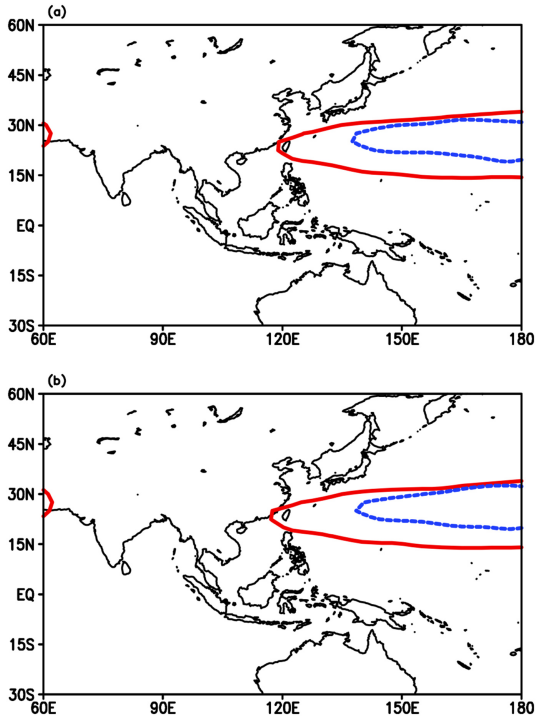

Figure 8. Composite lines of the summer 5870 gpm in 500 hPa for high (solid line) and low (short dotted line) $R_{WNP/BOB}$ **(a)** and $R_{WNP/SCS}$ **(b)**.

the equatorial Indian Ocean/Maritime Continent associated with Indian Ocean–western Pacific warming have favored the westward extension of the WPSH since the late 1970s. Therefore, the decadal trend of the SST in the Indian Ocean, the western Pacific, and the equatorial central-eastern Pacific is associated with the decadal trend of the WPSH, the $R_{WNP/BOB}$, and the $\delta^{18}O_{cs}$ in East Asia.

6 Discussions and conclusions

To verify our results of the variability of the relative intensities of the WVTs and their relationship with atmospheric circulation, we use the ERA-40 reanalysis data to repeat the analysis. The result shows that both $R_{WNP/BOB}$ and $R_{WNP/SCS}$ from the ERA-40 have significant correlations of 0.95 with those from the NCEP/NCAR reanalysis for the years 1960–1994. The atmospheric circulations, the WVT, and the SST associated with $R_{WNP/BOB}$ and $R_{WNP/SCS}$ are also consistent with those from the NCEP/NCAR reanalysis.

The relative intensities of the WVTs from the western North Pacific and the Bay of Bengal to East Asia experienced a decadal trend, which was recorded by the $\delta^{18}O_{cs}$. Based on the assumption of the "circulation effect" from Tan (2009, 2014), the $\delta^{18}O_{cs}$ value is primarily controlled by the relative portion variation of the local and remote WVTs. The decadal increase occurs in the time series of $R_{WNP/BOB}$ and

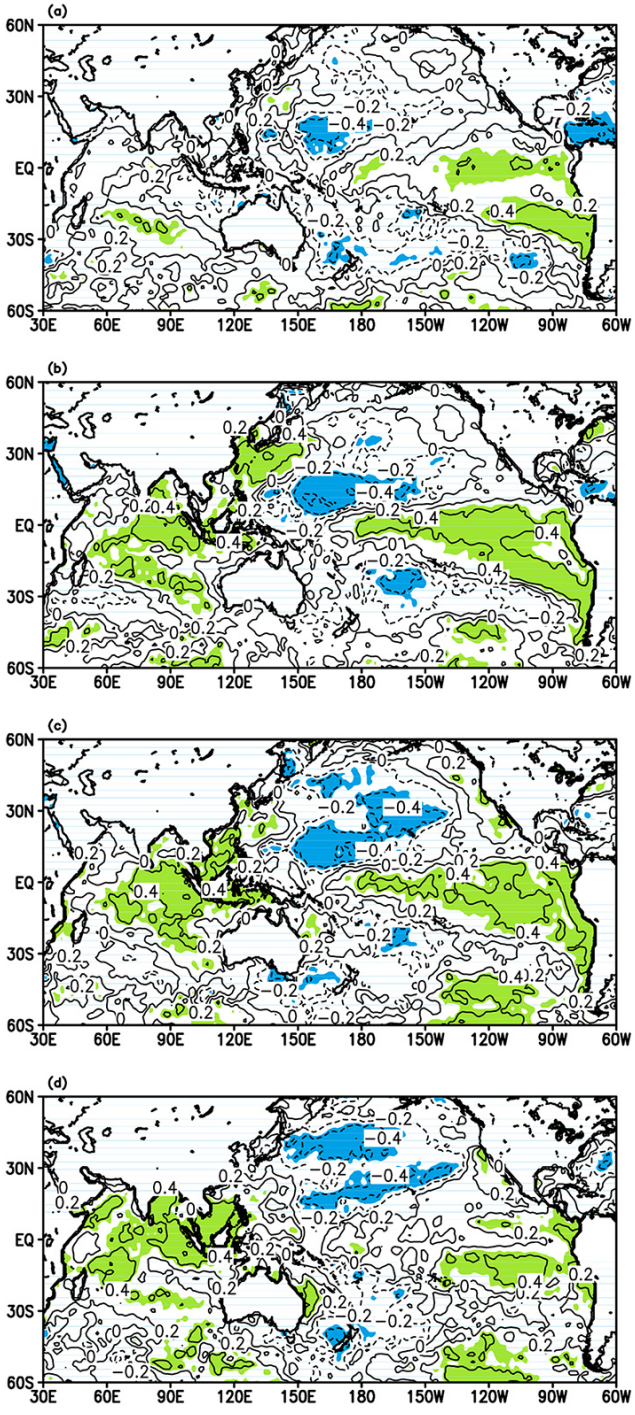

Figure 9. Correlation maps of the summer $R_{WNP/BOB}$ with the SST in the previous autumn (September-October-November) **(a)**, winter (December-January-February) **(b)**, spring (March-April-May) **(c)**, and concurrent summer (June-July-August) **(d)** for 1960–1994. The shaded area is above the 95 % confidence level.

$R_{WNP/SCS}$, most likely resulting from the strengthening of the WVT from the western North Pacific. In high $R_{WNP/BOB}$ years, the Asian low weakens, and the WPSH extends westward; subsequently, the WVT from the western North Pacific to East Asia increases because of the strengthening of the easterly winds to the south of the WPSH. The westerly and southwesterly winds from the Bay of Bengal to East Asia decrease, and the WVT from the Bay of Bengal to East Asia weakens. The atmospheric circulations and the WVTs associated with $R_{WNP/SCS}$ are similar to those associated with $R_{WNP/BOB}$. For high $R_{WNP/SCS}$ years, the WVT from the western North Pacific to East Asia strengthens, and the WVT from the South China Sea weakens.

$R_{WNP/BOB}$ and $R_{WNP/SCS}$ are closely related to the preceding SST. When the equatorial central-eastern Pacific is in the El Niño phase, the SST in the tropical Indian Ocean, the Bay of Bengal, and the South China Sea is high; the SST at the middle latitudes in the North Pacific is low; and $R_{WNP/BOB}$ and $R_{WNP/SCS}$ tend to be high. Previous studies have indicated that the WPSH is an important circulation system, influencing climate and weather in East Asia, and is closely related to the SST in the equatorial central-eastern Pacific and the tropical Indian Ocean (Wang et al., 2000; Lau and Nath, 2009; Yang et al., 2007; Xie et al., 2009). In addition, $R_{WNP/BOB}$ and $R_{WNP/SCS}$ are closely related to the position and intensity of the WPSH. When $R_{WNP/BOB}$ and $R_{WNP/SCS}$ are high, the WPSH extends westwards. Therefore, the SST in the equatorial central-eastern Pacific and the tropical Indian Ocean are most likely related to $R_{WNP/BOB}$ and $R_{WNP/SCS}$ through the WPSH and subsequently affect the $\delta^{18}O_p$, which is inherited or recorded by the $\delta^{18}O_{cs}$.

The Supplement related to this article is available online at doi:10.5194/cp-10-975-2014-supplement.

Acknowledgements. We thank the Climate Diagnostic Center/NOAA for providing the NCEP/NCAR reanalysis data and the Hadley Centre, Met Office for providing monthly mean HadISST data on its website. Thanks also to Yaoqi He for providing the data of the stalagmite isotope series D15. We also would like to thank the editor and two anonymous reviewers for improving the original manuscript. This work was jointly sponsored the National Natural Science Foundation of China (41030103, 41205057), the CAS Strategic Priority Research Program (grant XDA05080501), and the Basic Research Operation Foundation of the Chinese Academy of Meteorological Sciences (2013Z004).

Edited by: D. Fleitmann

References

Araguás-Araguás, L., Froehlich, K., and Rozanski, K.: Stable isotope composition of precipitation over southeast Asia, J. Geophys. Res., 103, 28721–28742, 1998.

Clemens, S. C., Prell, W. L., and Sun, Y.: Orbital-scale timing and mechanisms driving Late Pleistocene Indo–Asian summer monsoons: Reinterpreting cave speleothem δ^{18}O, Paleoceanography, 25, PA4207, doi:10.1029/2010PA001926, 2010.

Cosford, J., Qing, H., Eglington, B., Mattey, D., Yuan, D., Zhang, M., and Cheng, H.: East Asian monsoon variability since the Mid-Holocene recorded in a high-resolution, absolute-dated aragonite speleothem from eastern China, Earth Planet. Sc. Lett., 275, 296–307, 2008.

Dansgaard, W.: Stable isotopes in precipitation, Tellus, 16, 436–468, 1964.

Dayem, K. E., Molnar, P., Battisti, D. S., and Roe, G. H.: Lessons learned from oxygen isotopes in modern precipitation applied to interpretation of speleothem records of paleoclimate from eastern Asia, Earth Planet. Sc. Lett., 295, 219–230, 2010.

Ding, Y., Wang, Z., and Sun, Y.: Inter-decadal variation of the summer precipitation in East China and its association with decreasing Asian summer monsoon, Part I: Observed evidences, Int. J. Climatol., 28, 1139–1161, 2008.

Frappier, A. B.: Masking of interannual climate proxy signals by residual tropical cyclone rainwater: Evidence and challenges for low-latitude speleothem paleoclimatology, Geochem. Geophy. Geosy., 14, 3632–3647, 2013.

Gong, D. and He, X.: Interdecadal Change in Western Pacific Subtropical High and Climatic Effects, Acta Geogra Phica Sin., 57, 185–193, 2002.

He, Y., Wang, Y., Kong, X., and Cheng, H.: High resolution stalagmite δ^{18}O records over the past 1000 years from Dongge Cave in Guizhou, Chinese Sci. Bull., 50, 1003–1008, 2005.

Hu, C., Henderson, G. M., Huang, J., Xie, S., Sun, Y., and Johnson, K. R.: Quantification of Holocene Asian monsoon rainfall from spatially separated cave records, Earth Planet. Sc. Lett., 266, 221–232, 2008.

Hu, Z. Z.: Interdecadal variability of summer climate over East Asia and its association with 500 hPa height and global sea surface temperature, J. Geophys. Res., 102, 19403–19412, 1997.

Jiang, X. and Li, Y.: The review of water vapor transportation and its effects on drought and flood over China, Sci. Meteorol. Sin., 29, 138–142, 2009.

Johnson, K. R. and Ingram, B. L.: Spatial and temporal variability in the stable isotope systematics of modern precipitation in China: implications for paleoclimate reconstructions, Earth Planet. Sc. Lett., 220, 365–377, 2004.

Kalnay, E., Kanamitsu, M., Kistler, R., Collins, W., Deaven, D., Gandin, L., Iredell, M., Saha, S., White, G., Woollen, J., Zhu, Y., Chelliah, M., Ebisuzaki, W., Higgins, W., Janowiak, J., Mo, K. C., Ropelewski, C., Wang, J., Leetmaa, A., Reynolds, R., Jenne, R., and Joseph, D.: The NCEP/NCAR 40-year reanalysis project, B. Am. Meteorol. Soc., 77, 437–471, 1996.

Kilbourne, H. K., Biasatti, D., and Cooper, W. L.: Tropical Cyclone Reconstruction Implications of Hurricane Irene Precipitation δ^{18}O Anomalies and Their Transfer into Oysters in the Chesapeake Bay Region, August 2011, Fallmeeting, Session: PP33A: Climate Variability From High-Resolution Proxies III Posters, PP33A-2104, AGU, San Francisco, 2012.

Lau, K. M. and Li, M. S.: The monsoon of East Asia and its global associat ions – A survey, B. Am. Meteorol. Soc., 65, 114–125, 1984.

Lau, N. C. and Nath, M. J.: A Model Investigation of the Role of Air–Sea Interaction in the Climatological Evolution and ENSO-Related Variability of the Summer Monsoon over the South China Sea and Western North Pacific, J. Climate, 22, 4771–4792, 2009.

Lee, J. E., Risi, C., Worden, J., Scheepmaker, R. A., Lintner, B., and Frankenberg, C.: Asian monsoon hydrometeorology from TES and SCIAMACHY water vapor isotope measurements and LMDZ simulations: Implications for speleothem climate record interpretation, J. Geophys. Res., 117, D15112, doi:10.1029/2011JD017133, 2012.

Li, H. C., Ku, T. L., Stott, L. D., and Chen, W. J.: Applications of interannual-resolution stable isotope records of speleothem: climatic changes in Beijing and Tianjin, China, Sci. China, 41, 362–368, 1998.

Liu, J. R., Song, X. F., Yuan, G. F., Sun, X. M., Liu, X., and Wang, S. Q.: Characteristics of δ^{18}O in precipitation over Eastern Monsoon China and the water vapor sources, Chinese Sci. Bull., 55, 200–211, 2010.

Liu, J. H., Zhang, P. Z., Cheng, H., Chen, F. H., Yang, X. L., Zhang, D. Z., Zhou, J., Jia, J. H., An, C. L., Sang, W. C., and Johnson, K. R.: Asian summer monsoon precipitation recorded by stalagmite oxygen isotopic composition in the western Loess Plateau during AD1875–2003 and its linkage with ocean-atmosphere system, Chinese Sci. Bull., 53, 2041–2049, 2008.

Liu, Z., Wen, X., Brady, E. C., Otto-Bliesner, B., Yu, G., Lu, H., Cheng, H., Wang, Y., Zheng, W., Ding, Y., Edwards, R. L., Cheng, J., Liu, W., and Yang, H.: Chinese cave records and the East Asia Summer Monsoon, Quaternary Sci. Rev., 83, 115–128, 2014.

Lu, R. and Ye, H.: Inter-annual and seasonal changes of the West Pacific subtropical high, in: The progress and application of the new research on the Western Pacific subtropical high, edited by: He, J., Qi. L., and Zhang, R., Meteorological Press, Beijing, 2010.

Ma, Z. B., Cheng, H., Tan, M., Edwards, R. L., Li, H. C., You, C. F., Duan, W. H., Wang, X., and Kelly, M. J.: Timing and structure of the Younger Dryas event in northern China, Quaternary Sci. Rev., 41, 83–93, 2012.

Maher, B. A.: Holocene variability of the East Asian summer monsoon from Chinese cave records: a re-assessment, Holocene, 18, 861–866, 2008.

Maher, B. A. and Thompson, R.: Oxygen isotopes from Chinese caves: records not of monsoon rainfall but of circulation regime, J. Quaternary Sci., 27, 615–624, doi:10.1002/jqs.2553, 2012.

O'Neil, J. R.: Theoretical and experimental aspects of isotopic fractionation, in: Stable Isotopes in High Temperature Geologic Processes, Reviews in Mineralogy, 16, edited by: Valley, J. W., Taylor Jr., H. P., and O'Neil, J. R., Mineralogical Society of America, Washington, D.C., 1–40, 1986.

Pausata, F. S. R., Battisti, D. S., Nisancioglu, K. H., and Bitz, C. M.: Chinese stalagmite δ^{18}O controlled by changes in the Indian monsoon during a simulated Heinrich event, Nat. Geosci., 4, 474–480, 2011.

Rayleigh, J. W. S.: Theoretical considerations respecting the separation of gases by diffusion and similar processes, Philos. Mag., 42, 493–498, 1896.

Rayner, N. A., Parker, D. E., Horton, E. B., Folland, C. K., Alexander, L. V., Rowell, D. P., Kent, E. C., and Kaplan, A.: A global analyses of sea surface temperature, sea ice, and night marine air temperature since the late nineteenth century, J. Geophys. Res., 108, 4407, doi:10.1029/2002JD002670, 2003.

Tan, L., Cai, Y., An, Z., Edwards, R. L., Cheng, H., Shen, C. C., and Zhang, H.: Centennial to decadal-scale monsoon precipitation variability in the semi-humid region, northern China during the last 1860 years: Records from stalagmites in Huangye Cave, Holocene, 21, 287–296, 2011.

Tan, L., Cai, Y., Cheng, H., An, Z., and Edwards, R. L.: Summer monsoon precipitation variations in central China over the past 750 years derived from a high-resolution absolute-dated stalagmite, Palaeogeogr. Palaeocl., 280, 432–439, 2009.

Tan, M.: Circulation effect: Climatic significant of the short term variability of the oxygen isotopes in stalagmites from monsoonal China – Dialogue between paleoclimate records and modern climate research, Quaternary Sci., 29, 851–862, 2009.

Tan, M.: Circulation effect: response of precipitation δ^{18}O to the ENSO cycle in monsoon regions of China, Clim. Dynam., 42, 1067–1077, doi:10.1007/s00382-013-1732-x, 2014.

Tan, M., Liu, T., Hou, J., Qin, X., Zhang, H., and Li, T.: Cyclic rapid warming on centennial-scale revealed by a 2650-year stalagmite record of warm season temperature, Geophys. Res. Lett., 30, 1617–1620, 2003.

Tao, S. Y. and Chen, L. X.: A review of recent research on the east Asian summer monsoon in China, in: Review of Monsoon Meteorology, edited by: Chang, C. P. and Krishnamurti, T. N., Oxford Univ. Press, New York, 60–92, 1987.

Tian, H., Guo, P., and Lu, W.: Characteristic of vapor inflow corridors related to summer rainfall in China and impact factors, J. Trop. Meteorol., 20, 401–408, 2004.

Tian, L., Yao, T., Schuster, P. F., White, J. W. C., Ichiyanagi, K., Pendall. E., Pu, J., and Yu, W.: Oxygen-18 concentrations in recent precipitation and ice cores on the Tibetan Plateau, J. Geophys. Res., 108, 4293, doi:10.1029/2002JD002173, 2003.

Wang, B., Xiang, B., and Lee, J. Y.: Subtropical high predictability establishes a promising way for monsoon and tropical storm predictions, P. Natl. Acad. Sci., 110, 2718–2722, 2013.

Wang, B., Wu, R., and Fu, X.: Pacific–East Asian teleconnection: How does ENSO affect East Asian climate?, J. Climate, 13, 1517–1536, 2000.

Wang, Y., Cheng, H., Edwards, R. L., An, Z., Wu, J., Shen, C., and Dorale, J. A.: High-Resolution Absolute-Dated Late Pleistocene Monsoon Record from Hulu Cave, China, Science, 294, 2345–2348, 2001.

Xie, S. P., Hu, K., Hafner, J., Tokinaga, H., Du, Y., Huang, G., and Sampe, T.: Indian Ocean capacitor effect on Indo–western Pacific climate during the summer following El Niño, J. Climate, 22, 730–747, 2009.

Yamanaka, T., Shimada, J., Hamada, Y., Tanaka, T., Yang, Y., Zhang, W., and Hu, C.: Hydrogen and oxygen isotopes in precipitation in the northern part of the North China Plain: climatology and interstorm variability, Hydrol. Process., 18, 2211–2222, 2004.

Yang, J., Liu, Q., Xie, S. P., Liu, Z., and Wu, L.: Impact of the Indian Ocean SST basin mode on the Asian summer monsoon, Geophys. Res. Lett., 34, L02708, doi:10.1029/2006GL028571, 2007.

Yuan, D., Cheng, H., Edwards, R. L., Dykoski, C. A., Keelly, M. J., Zhang, M., Qing, J., Lin, Y., Wang, Y., Wu, J., Dorale, J. A., An, Z., and Cai, Y.: Timing, Duration, and Transitions of the Last Interglacial Asian Monsoon, Science, 304, 575–578, 2004.

Zhang, P., Cheng, H., Edwards, R. L., Chen, F., Wang, Y., Yang, X., Liu, J., Tan, M., Wang, X., Liu, J., An, C., Dai, Z., Zhou, J., Zhang, D., Jia, J., Jin, L., and Johnson, K. R.: A Test of Climate, Sun, and Culture Relationships from an 1810-Year Chinese Cave Record, Science, 322, 940–942, 2008.

Zhang, R.: Relations of water vapor transport from Indian monsoon with that over East Asia and the summer rainfall in China, Adv. Atmos. Sci., 18, 1005–1017, 2001.

Zheng, Y., Zhong, W., Peng, X., Xue, J., Zhao, Y., Ma, Q., and Cai, Y.: Correlation of δ^{18}O in precipitation and moisture sources at Yunfu, Western Guangdong Province, China, Environ. Sci., 30, 637–643, 2009.

Zhou, T.: Comparison of the global air-sea freshwater exchange evaluated from independent data sets, Prog. Natural Sci., 13, 626–631, 2003.

Zhou, T., Yu, R., Zhang, J., Drange, H., Cassou, C., Deser, C., Hodson, D. L. R., Sanchez-Gomez, E., Li, J., Keenlyside, N., Xin, X., and Okumura, Y.: Why the Western Pacific subtropical high has extended westward since the late 1970s, J. Climate, 22, 2199–2215, 2009.